Synchrotron radiation X-ray fluorescence analysis of biodistribution and pulmonary toxicity of nanoscale titanium dioxide in mice

Article *in* The Analyst · August 2013

DOI: 10.1039/c3an01267k · Source: PubMed

8 authors, including:

Jichao Zhang
Shanghai Institute of Applied Physics
15 PUBLICATIONS **215** CITATIONS
SEE PROFILE

Bo Li
Jilin University
11 PUBLICATIONS **212** CITATIONS
SEE PROFILE

Xiaohan Yu
Shanghai Institute of Applied Physics
55 PUBLICATIONS **621** CITATIONS
SEE PROFILE

Qing Huang
174 PUBLICATIONS **10,937** CITATIONS
SEE PROFILE

IF : 3.906

Analyst

RSC Publishing

PAPER

View Article Online
View Journal | View Issue

Cite this: *Analyst*, 2013, **138**, 6511

Synchrotron radiation X-ray fluorescence analysis of biodistribution and pulmonary toxicity of nanoscale titanium dioxide in mice

Jichao Zhang,[a] Bo Li,*[ab] Yi Zhang,[a] Aiguo Li,[a] Xiaohan Yu,*[a] Qing Huang,[a] Chunhai Fan[a] and Xiaoqing Cai*[a]

Received 2nd July 2013
Accepted 3rd August 2013

DOI: 10.1039/c3an01267k

www.rsc.org/analyst

Using synchrotron radiation X-ray fluorescence (SRXRF), we have examined the biodistribution and pulmonary toxicity of nanoscale titanium dioxide (nanoTiO_2) in mice at the elemental level. Notably, nanoTiO_2 particles were mainly retained in lungs after intratracheal instillation, slowly cleared and were still present at 3 months. Different methods of intratracheal instillation influenced the clearance of nanoTiO_2 from lungs. NanoTiO_2 interfered with the natural distribution of K, Ca, Fe, Cu and Zn in lungs. We have thus demonstrated that SRXRF provides an effective approach to investigate the distribution of metal nanomaterials and native metal elements in tissues and organs, which offers new opportunities for revealing nanotoxic mechanisms of nanomaterials.

Introduction

Nanotechnology, as a newly emerging science, presents many opportunities and benefits for new materials with significantly improved properties as well as revolutionary applications in various fields including energy, environment, medicine, *etc.*[1] However, concerns over adverse and unanticipated effects on human health have also been raised. The unique characteristics of nanomaterials that are essential for successful application might also lead to negative health impacts.[2] It was reported that inhaled nanoparticles (<100 nm) had a special biological mechanism and led to maximum deposition in lungs.[3] Therefore, it is very important to evaluate the pulmonary toxicity of nanomaterials accompanied by their application.

Nanoscale titanium dioxide (nanoTiO_2), due to its special physicochemical characteristics, has been widely used as a photocatalyst in air and water cleaning,[4] sunscreens and cosmetics,[5] special coatings and paints.[6,7] However, studies with respect to pulmonary toxicology of nanoTiO_2 have never stopped. Previous studies indicate that nanoTiO_2 could induce acute pulmonary inflammatory responses such as pulmonary emphysema, macrophage accumulation, extensive disruption of alveolar septa, type II pneumocyte hyperplasia, and epithelial cell apoptosis.[8] The toxic effect of nanoTiO_2 is dose-dependent, and correlates well with the crystal form[9] and surface treatments.[10] There are controversial views with regard to the influence of size (surface area).[11,12] Further study suggests that cell cycle, apoptosis, chemokine, and complementary pathways may be involved in nanoTiO_2-induced pulmonary toxicity.[8] However, the toxicity mechanism of nanoTiO_2 has not been completely clarified.

So far, SRXRF has been widely used for elemental analysis in biomedicine, material and environmental sciences. Using an X-ray fluorescence microprobe provided by third generation synchrotron radiation sources, SRXRF can obtain the distribution of elements in biological samples with higher sensitivity and resolution. Compared with ICP/MS, SRXRF is a multi-elemental analytical technique, and does not destroy the irradiated samples.[13,14] Meanwhile, it makes it possible to detect the elemental distribution in different regions of various sections. By using SRXRF, Kemner *et al.* observed the distribution of the Cr element in *Pseudomonas fluorescens* after exposure to potassium dichromate solution for 6 hours;[15] Finney *et al.* revealed large-scale relocalization and extracellular translocation of cellular copper during angiogenesis;[16] Korbas *et al.* observed organomercury uptake and accumulation in zebrafish larvae at the tissue and cellular level.[17]

SRXRF makes it possible for toxicologists to study the toxicology of nanoTiO_2. The content of the Ti element in organs may be used to evaluate the biological behavior of nanoTiO_2. Furthermore, the effect of nanoTiO_2 on the distribution of other metal elements in lungs contributes to an examination of the pulmonary toxicity of nanoTiO_2 at the elemental level. It is well known that metal elements, such as K, Ca, Fe, Cu and Zn, are essential for living organisms and exhibit important biological significance. The abnormal distribution of these metal elements in organisms may be involved in the occurrence and development of some diseases.[18–20] The evaluation of metal

[a]*Division of Physical Biology, Department of Materials and Energy Sciences & Bioimaging Center, Shanghai Synchrotron Radiation Facility, Shanghai Institute of Applied Physics, Chinese Academy of Sciences, Shanghai 201800, China. E-mail: Caixiaoqing@sinap.ac.cn; libosf@gmail.com; yuxiaohan@sinap.ac.cn*

[b]*Department of Human Anatomy, College of Basic Medical Sciences, Jilin University, Changchun, 130021, China*

element distribution combined with pathological changes in lungs may contribute to further elucidating the mechanism of pulmonary toxicity induced by nanoTiO_2.

In the present study, we investigate the distribution of intratracheally instilled nanoTiO_2 and its effect on native metal elements using SRXRF to directly image metal localization in organs of mice. Herein, we find that nanoTiO_2 particles are mainly retained in lungs after intratracheal instillation, are slowly cleared and are still present at three months. The detailed procedure used during instillation influenced nanoTiO_2 clearance from lungs. NanoTiO_2 increases the content of K, Ca, Fe, Cu and Zn. These results indicate that SRXRF is useful to determine the distribution of metal nanomaterials and reveal their toxic mechanisms.

Materials and methods

Characterization of nanoTiO_2

NanoTiO_2 (20 nm) was purchased from Shanghai Hujing Sub-Nanoscale New Material Co. Ltd., Shanghai, China. Prior to animal experiments, its particle size was analyzed by a transmission electron microscope (TEM); its crystal form was determined by a powder X-ray diffractometer (XRD, D/MAX-2550-18KW); its composition was analyzed *via* its energy spectrum by a scanning electron microscope (SEM, LEO 1530VP).

Animals

All animal experiments were performed in compliance with the local ethics committee. Male C57BL/6 mice (18–22 g) were obtained from the Shanghai Slack Experimental Animal Center. The animal room was maintained at 22 °C with a daily light–dark cycle (06:00–18:00 light). Mice were fed standard mice chow and provided water *ad libitum*. All the procedures using animals were reviewed and approved by the Institutional Animal Care and Use Committee.

Intratracheal instillation

To evaluate the biodistribution of nanoTiO_2 and its pulmonary toxicity at the elemental level, the mice were intratracheally instilled with 1 mg kg^{-1} nanoTiO_2 (using 0.2 mg ml^{-1} suspension) and terminated at 1 day, 1 week, 1 month and 3 months. The general procedure was modified from previous experiments.[21,22] Briefly, mice were anesthetized with an intraperitoneal injection of 50 mg kg^{-1} pentobarbital sodium (10 mg ml^{-1}; Sigma, St. Louis, MO) and placed in a supine position head up on a board tilted at 50°. A midline incision was performed in the neck and the trachea was exposed. The solution was drawn (up to a premarked location) into a 0.45 mm intravenous infusion needle and rapidly instilled into the lungs with a 1 ml plastic disposable syringe prefilled with 100 μl air. After intratracheal instillation, the mice were placed in a vertical position and rotated for 0.5–1 min to distribute the instillation evenly within the lungs. The neck incision was then sutured. The mice recovered and were active within 20 min after intratracheal instillation.

Preparation of sections

After the mice were exsanguinated and sacrificed by removing their eyes, the whole lung, liver and spleen were collected, embedded in OCT compound and frozen in liquid nitrogen. Subsequently, the isolated organs were sectioned on a cryotome. Of two adjacent sections, one (5 μm thickness) was mounted on a glass slide and stained with hematoxylin and eosin for pathological observation, and the other (20 μm thickness), designed for synchrotron radiation X-ray fluorescence imaging, was fixed on 3 μm thick Mylar films (polycarbonate film) and dried at room temperature.

X-ray fluorescence imaging

Samples were analyzed at the BL15U1 hard X-ray microprobe at the Shanghai Synchrotron Radiation Facility (SSRF). A schematic representation of the scanning XRF microprobe setup[23] is shown in Fig. 1. A Si (111) double crystal was applied to monochromatize the continuous synchrotron X-ray from an undulator X-ray source. Samples were placed on a 7-axis stage with a high spatial resolution of 0.1 μm in x, y and z directions. The incident X-ray irradiated on the samples at 45°, and a 50 mm^2 silicon-drift detector (Vortex, USA) placed at 90° from the incident beam was used to collect the X-ray fluorescence spectrum. A light microscope connected with a computer was used to monitor the samples. The incident X-ray energy was set to 10 keV to excite the fluorescence of K, Ca, Fe, Cu and Zn elements. The cross-section size of the beam was adjusted to about 100 × 100 μm^2. The samples were raster-scanned in steps of 100 μm for x and z directions. The scan time was 1 second per pixel and about 8 h for the whole section (12 mm × 12 mm).

Data analysis

The X-ray spectra were fitted using the PyMCA toolkit. The Compton scattering in the SRXRF spectrum was utilized as an internal standard to compensate the differences in thickness and density of thin tissue sections.[18,24] And the standard reference materials of bovine liver (NIST 1577a) and trace elements in glass (NIST 612) were used to calculate the quantitative concentration of K, Ca, Ti, Fe, Cu and Zn in samples. The concentration distribution of all elements was processed to 2-dimensional elemental maps of images with false coloring using plot2d.py software. The average content of metal elements in sections of lungs was calculated by subtracting the pixels outside of the tissue.

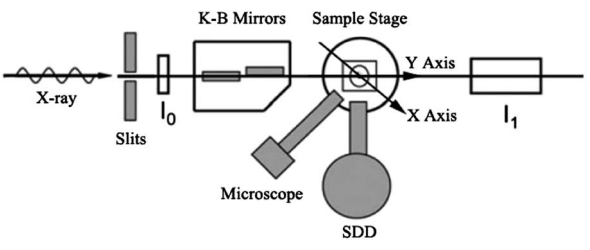

Fig. 1 A schematic representation of the scanning XRF microprobe setup at BL15U1.

Results and discussion

Characterization of nanoTiO$_2$

As shown in Fig. 2A, the primary size of nanoTiO$_2$ is about 20 nm and is consistent with the manufacturer-supported information. The result of XRD indicates that its crystal form is anatase (Fig. 2B). Meanwhile, the SEM energy spectrum was used to analyze the composition of nanoTiO$_2$. By this method, only O, Si and Ti elements were obviously detected (the Si element originates from silicon-slice supporting samples), suggesting that the nanoTiO$_2$ sample is pure (Fig. 2C).

NanoTiO$_2$ particles were mainly retained in lungs after intratracheal instillation, slowly cleared and still present at 3 months

The biodistribution pattern of nanoTiO$_2$ was determined by exposing each mouse to 1 mg kg^{-1} nanoTiO$_2$ (using 0.2 mg ml^{-1} suspension) with intratracheal instillation for 1 day before imaging. Fig. 3 shows the images of the Ti element in sections of different organs including lungs, liver and spleen. The images clearly show the higher fluorescence intensity in a section of lung and a small amount in liver and spleen, indicating that nanoTiO$_2$ particles mainly stay in lungs after intratracheal instillation. This result is consistent with the previous study.[20] Furthermore, it is observed that Ti deposition in lungs is not homogeneous and mostly locates in the upper part of the left lung. The regional distribution of nanoTiO$_2$ in sections of lungs may be related to many factors including different respiratory phases of mice during instillation.

Additional detailed quantitative information about nanoTiO$_2$ distribution in lungs was obtained by imaging the sections with different exposure times. The mice were exposed to 1 mg kg^{-1} nanoTiO$_2$ by intratracheal instillation for 1 day, 1 week, 1 month and 3 months. Following the exposure the sections of lungs were prepared for imaging. Fig. 4 compares the quantitative Ti level in representative sections of lungs at these four time points. The concentration of the Ti element is about 216.3 μg g^{-1} at 1 day, 160.8 μg g^{-1} at 1 week, and 128.6 μg g^{-1} at

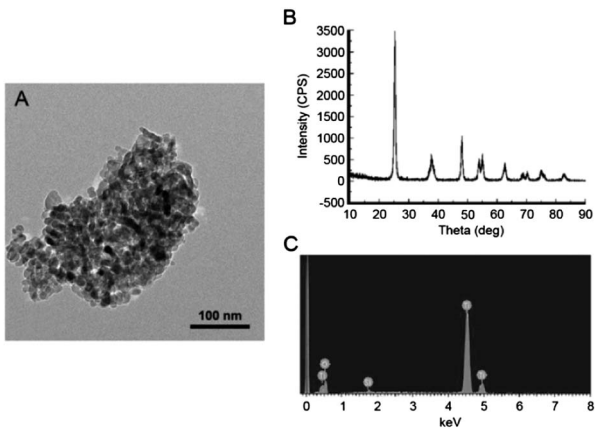

Fig. 2 Characterization of nanoTiO$_2$. (A) TEM image of nanoTiO$_2$. (B) Crystal form of nanoTiO$_2$ by XRD. (C) The energy spectrum of nanoTiO$_2$ by SEM.

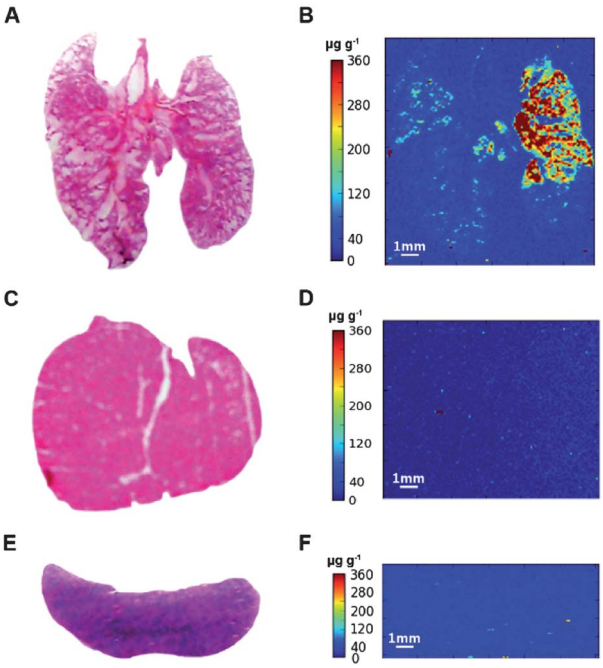

Fig. 3 Distribution of the Ti element in sections of lungs (A and B), liver (C and D) and spleen (E and F) after 1 day exposure with 1 mg kg^{-1} nanoTiO$_2$. Each X-ray fluorescence image (right) is paired with its respective histological image (left) with hematoxylin–eosin staining.

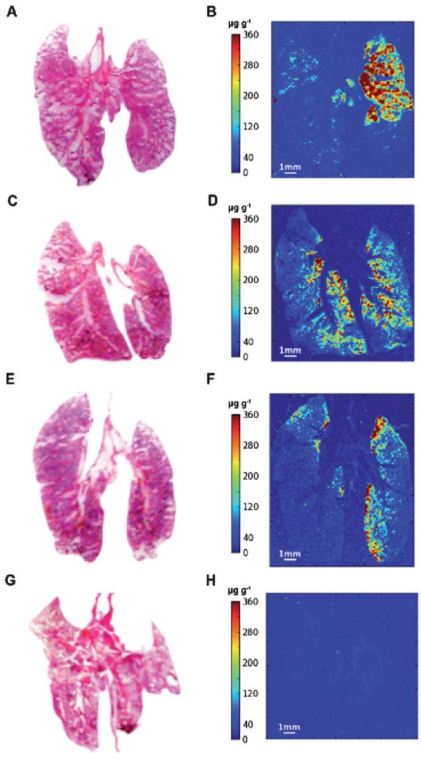

Fig. 4 Distribution of the Ti element in sections of lungs at 1 day (A and B), 1 week (C and D), 1 month (E and F) and 3 months (G and H) following exposure with 1 mg kg^{-1} nanoTiO$_2$. Each X-ray fluorescence image (right) is paired with its respective histological image (left) with hematoxylin-eosin staining.

1 month and remained 78.9 μg g^{-1} at 3 months, indicating that nanoTiO$_2$ particles are slowly cleared from lungs. NanoTiO$_2$ may be taken up and cleared by alveolar macrophages.[24] Meanwhile, the lower Ti level at 3 months implies the persistence of nanoTiO$_2$.

Differences in intratracheal instillation methods influence the clearance of nanoTiO$_2$ from lungs

To investigate whether nanoTiO$_2$ clearance from lungs is related to the instillation procedure, the nanoTiO$_2$ aqueous solution (1 mg kg^{-1}, using 0.2 mg ml^{-1} suspension) was intratracheally instilled into the lungs using a 1 ml syringe prefilled with or without 100 μl air. Fig. 5 compares Ti distribution in sections of lungs at 1 month with different methods of instillation. The section of lungs instilled with extra air shows a higher level of Ti (≈128.6 μg g^{-1}), comparable with the level found in the section instilled without air (≈93.6 μg g^{-1}), suggesting that different methods of instillation through the trachea can affect the clearance of nanoTiO$_2$ from lungs. Meanwhile, higher concentration of Ti locates at the medial border of lungs instilled with air (Fig. 5C), and near the hilum of lungs instilled without air (Fig. 5D). In addition, the histopathological observation shows that the extra instilled air promotes more nanoTiO$_2$ particles from the bronchia into the alveolar spaces at 1 day (Fig. 5E and F). These results imply that the clearance of nanoTiO$_2$ may be involved in its intrapulmonary distribution. Compared with that instilled with air, more nanoTiO$_2$ particles locate in the bronchia of lungs instilled without air and may be cleared by alveolar macrophages.

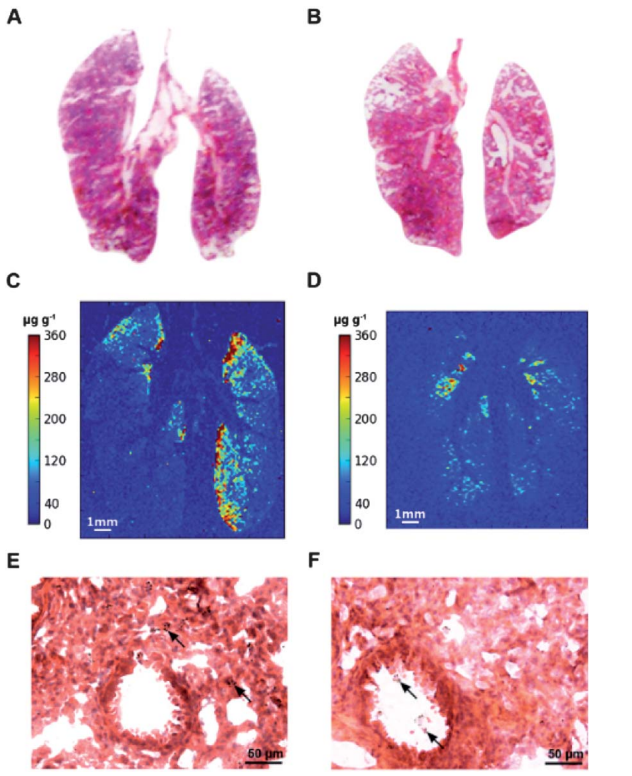

Fig. 5 Influence of different instilled methods on clearance of nanoTiO$_2$ from lungs. NanoTiO$_2$ aqueous solution (1 mg kg^{-1}) was intratracheally instilled into lungs with (A, C, and E) or without (B, D, and F) 100 μl air. (A and B) Histological images of lungs at 1 month following exposure. (C and D) X-ray fluorescence images of lungs at 1 month following exposure. (E and F) Histopathological observation of lungs at 1 day following exposure.

NanoTiO$_2$ interferes with the natural distribution of K, Ca, Fe, Cu and Zn in lungs

Fig. 6 shows quantitative elemental distribution in representative sections of nanoTiO$_2$ exposed and unexposed lungs. The sections of lungs treated with nanoTiO$_2$ show more or less increase in concentration of these elements at four time points compared with normal lungs, suggesting that nanoTiO$_2$ influences their spatial distribution in lungs. Table 1 presents detailed information on the content of metal elements in lungs. Compared with normal lungs (≈3.14 mg g^{-1}), the K level increases gradually from 1 day (≈4.17 mg g^{-1}), reaches a peak at 1 month (≈4.66 mg g^{-1}), and then declined at 3 months (≈2.34 mg g^{-1}). The Ca level shows the same variation tendency with time as K. Meanwhile, the peaks of Fe, Cu and Zn levels arise at 1 day (≈0.33 mg g^{-1}, 13.7 μg g^{-1} and 71.5 μg g^{-1} respectively), and then decrease until 3 months.

The elevated contents of metal elements may be closely related to the nanoTiO$_2$-induced pulmonary responses characterized by the accumulation of alveolar macrophages and infiltration of neutrophils in the alveolar spaces.[8,26] It is well known that macrophages and neutrophils contain a certain amount of metal elements including K, Ca, Fe, Cu and Zn. K and Ca are the major intracellular elements, and their ionic levels are correlated with the migration of macrophages and neutrophils.[27–31] Fe is stored in ferritin within macrophages and lactoferrin within neutrophils.[32,33] Lactoferrin may play an integral role in the innate immune response of the neutrophil to microbial infection. Cu and Zn, as co-factors for many known enzymes, are critically involved in the function of macrophages and neutrophils.[34–38] Moreover, the effusion of red cells may contribute to the elevation of the Fe content.

The decreased levels of metal elements may mainly depend on the phagocytosis and clearance of alveolar macrophages. Accompanied by the damage of epithelia and degranulation of neutrophils, the metal ions, metalloprotein and metalloprotease were released into the alveolar spaces. The released and extracellular metal ions may adsorb onto the surface of nanoTiO$_2$, and be phagocytized by alveolar macrophage.[39] Meanwhile, proteins or enzymes containing metal elements may experience the same fate. Finally, the majority of metal elements may be taken up and cleared by alveolar macrophages either through mucociliary clearance or other mechanisms.[25] In addition, a portion of the metal ions may enter the blood by passing through the air–blood barrier.

At the early phase of nanoTiO$_2$ exposure (1 day), the immigration of macrophages and neutrophils from blood into alveolar spaces through the air–blood barrier may lead to the elevation of regional metal element content. With the passage of time, the decreased levels of trace elements such as Fe, Cu and Zn may be due to the above clearance mechanism.

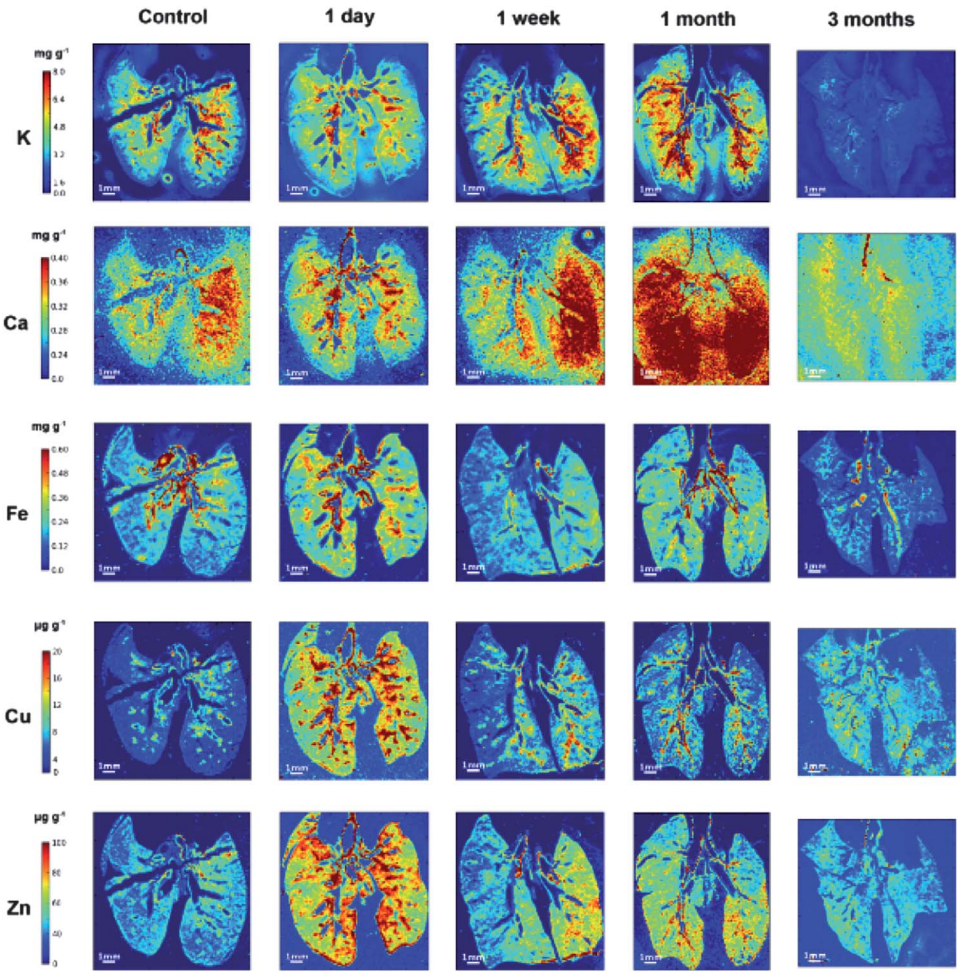

Fig. 6 Quantitative elemental distribution in nanoTiO$_2$ exposed and unexposed lungs. Comparison of metal elemental distributions for K, Ca, Fe, Cu and Zn in sections of lungs exposed to 1 mg kg^{-1} nanoTiO$_2$ for 1 day, 1 week, 1 month and 3 months with control lungs, measured using X-ray fluorescence imaging. Quantity of each element is plotted on the same scale for nanoTiO$_2$ exposed and unexposed sections.

Table 1 The average content of metal elements in sections of lungs

Elements	Control	1 day	1 week	1 month	3 months
K (mg g^{-1})	3.143	4.166	4.472	4.661	2.341
Ca (mg g^{-1})	0.290	0.291	0.310	0.390	0.298
Fe (mg g^{-1})	0.258	0.328	0.208	0.286	0.176
Cu (μg g^{-1})	5.690	13.71	10.45	12.34	9.437
Zn (μg g^{-1})	45.76	71.53	55.06	59.12	40.64

However, the continued cell infiltration and limited capability of clearance may induce the regional accumulation of major elements including K and Ca, and their levels increased gradually and reached a peak at one month. Subsequently, the reduced pulmonary inflammation accompanied by the elimination of nanoTiO$_2$ may account for their decreased levels.

Conclusions

SRXRF provides a novel approach to study the biological behavior of nanoTiO$_2$ in animals. The results are consistent with the previous study, indicating that SRXRF is suitable and effective for determining the distribution of metal nanomaterials. More importantly, SRXRF can provide spatial distribution images to show regional deposition and accumulation of these nanomaterials in tissues and organs without damage to samples, which is helpful to further investigate distribution patterns and reveal potential toxicity. Meanwhile, we also evaluated the nanoTiO$_2$-induced pulmonary response at the elemental level. The results show the effect of nanoTiO$_2$ on the distribution and content of metal elements, further demonstrating the pulmonary toxicity of nanoTiO$_2$. In addition, the changes of these elemental levels provide insight into revealing the toxic mechanism of nanoTiO$_2$. Our findings constitute a first step toward understanding the pulmonary toxicity of nanomaterials and their detailed mechanisms at the elemental level.

Acknowledgements

This work was supported by the Ministry of Science and Technology of China (2012CB825800, 2012CB932600,

2012CB825805), the National Natural Science Foundation of China (no. 11179004, 11275251, U1232113, U1232114, 31170077), K. C. Wong Education Foundation, and Youth Innovation Promotion Association CAS.

References

1 R. F. Service, *Science*, 2004, **304**, 1732–1734.
2 B. Fadeel, V. Kagan, H. Krug, A. Shvedova, M. Svartengren, L. Tran and L. Wiklund, *Nanotoxicology*, 2007, **1**, 73–84.
3 P. G. A. Rogueda and D. Traini, *Expert Opin. Drug Delivery*, 2007, **4**, 595–606.
4 D. Sun, T. T. Meng, T. H. Loong and T. J. Hwa, *Water Sci. Technol. Libr.*, 2004, **49**, 103–110.
5 G. Wakefield and J. Stott, *J. Cosmet. Sci.*, 2006, **57**, 385–395.
6 M. Guarino, A. Costa and M. Porro, *Bioresour. Technol.*, 2008, **99**, 2650–2658.
7 V. Kandavelu, H. Kastien and K. R. Thampi, *Appl. Catal., B*, 2004, **48**, 101–111.
8 H. W. Chen, S. F. Su, C. T. Chien, W. H. Lin, S. L. Yu, C. C. Chou, J. J. W. Chen and P. C. Yang, *FASEB J.*, 2006, **20**, 2393–2395.
9 D. B. Warheit, T. R. Webb, K. L. Reed, S. Frerichs and C. M. Sayes, *Toxicology*, 2007, **230**, 90–104.
10 D. B. Warheit, W. J. Brock, K. P. Lee, T. R. Webb and K. L. Reed, *Toxicol. Sci.*, 2005, **88**, 514–524.
11 G. Oberdorster, J. Ferin and B. E. Lehnert, *Environ. Health Perspect.*, 1994, **102**, 173–179.
12 D. B. Warheit, T. R. Webb, C. M. Sayes, V. L. Colvin and K. L. Reed, *Toxicol. Sci.*, 2006, **91**, 227–236.
13 C. J. Fahrni, *Curr. Opin. Chem. Biol.*, 2007, **11**, 121–127.
14 T. Paunesku, S. Vogt, J. Maser, B. Lai and G. Woloschak, *J. Cell. Biochem.*, 2006, **99**, 1489–1502.
15 K. M. Kemner, S. D. Kelly, B. Lai, J. Maser, E. J. O'Loughlin, D. Sholto-Douglas, Z. H. Cai, M. A. Schneegurt, C. F. Kulpa and K. H. Nealson, *Science*, 2004, **306**, 686–687.
16 L. Finney, S. Mandava, L. Ursos, W. Zhang, D. Rodi, S. Vogt, D. Legnini, J. Maser, F. Ikpatt, O. I. Olopade and D. Glesne, *Proc. Natl. Acad. Sci. U. S. A.*, 2007, **104**, 2247–2252.
17 M. Korbas, S. R. Blechinger, P. H. Krone, I. J. Pickering and G. N. George, *Proc. Natl. Acad. Sci. U. S. A.*, 2008, **105**, 12108–12112.
18 H. J. Wang, M. Wang, B. Wang, X. Y. Meng, Y. Wang, M. Li, W. Y. Feng, Y. L. Zhao and Z. F. Chai, *J. Anal. At. Spectrom.*, 2010, **25**, 328–333.
19 A. I. Bush, *Curr. Opin. Chem. Biol.*, 2000, **4**, 184–191.
20 B. van Ravenzwaay, R. Landsiedel, E. Fabian, S. Burkhardt, V. Strauss and L. Ma-Hock, *Toxicol. Lett.*, 2009, **186**, 152–159.
21 Y. L. Song, N. Fukuda, C. X. Bai, T. H. Ma, M. A. Matthay and A. S. Verkman, *J. Physiol.*, 2000, **525**, 771–779.
22 C. W. Lam, J. T. James, R. McCluskey and R. L. Hunter, *Toxicol. Sci.*, 2003, **77**, 126–134.
23 J. K. Qiu, B. A. Deng, Q. Yang, F. Yan, A. G. Li and X. H. Yu, *Nucl. Instrum. Methods Phys. Res., Sect. B*, 2011, **269**, 2662–2666.
24 L. M. Marco, E. D. Greaves and J. Alvarado, *Spectrochim. Acta, Part B*, 1999, **54**, 1469–1480.
25 M. Semmler-Behnke, S. Takenaka, S. Fertsch, A. Wenk, J. Seitz, P. Mayer, G. Oberdorster and W. G. Kreyling, *Environ. Health Perspect.*, 2007, **115**, 728–733.
26 E. Bermudez, J. B. Mangum, B. A. Wong, B. Asgharian, P. M. Hext, D. B. Warheit and J. I. Everitt, *Toxicol. Sci.*, 2004, **77**, 347–357.
27 D. Dal-Secco, T. M. Cunha, A. Freitas, J. C. Alves, F. O. Souto, S. Y. Fukada, R. Grespan, N. M. N. Alencar, A. F. Neto, M. A. Rossi, S. H. Ferreira, J. S. Hothersall and F. Q. Cunha, *J. Immunol.*, 2008, **181**, 4287–4298.
28 J. G. R. Elferink and B. M. de Koster, *Biochem. Pharmacol.*, 2000, **59**, 369–375.
29 K. H. Krause, K. P. Campbell, M. J. Welsh and D. P. Lew, *Clin. Biochem.*, 1990, **23**, 159–166.
30 R. M. Saraiva, M. O. Masuda and G. M. OliveiraCastro, *Braz. J. Med. Biol. Res.*, 1997, **30**, 1349–1357.
31 K. Toyama, T. Saito, Y. Fujiwara, O. A. Hatoum, D. D. Gutterman and H. Miura, *FASEB J.*, 2007, **21**, A854.
32 D. Goven, A. Boutten, V. Lecon-Malas, J. Marchal-Somme, P. Soler, J. Boczkowski and M. Bonay, *PLoS One*, 2010, **5**, e10886.
33 P. P. Ward, M. Mendoza-Meneses, P. W. Park and O. M. Conneely, *Am. J. Pathol.*, 2008, **172**, 1019–1029.
34 P. C. Joshi, R. Raynor, X. Fan and D. M. Guidot, *Am. J. Respir. Cell Mol. Biol.*, 2008, **39**, 218–226.
35 P. C. Joshi, A. Mehta, W. S. Jabber, X. Fan and D. M. Guidot, *Am. J. Respir. Cell Mol. Biol.*, 2009, **41**, 207–216.
36 C. White, J. Lee, T. Kambe, K. Fritsche and M. J. Petris, *J. Biol. Chem.*, 2009, **284**, 33949–33956.
37 U. Babu and M. L. Failla, *J. Nutr.*, 1990, **120**, 1692–1699.
38 U. Babu and M. L. Failla, *J. Nutr.*, 1990, **120**, 1700–1709.
39 P. Liang, Y. C. Qin, B. Hu, C. X. Li, T. Y. Peng and Z. C. Jiang, *Fresenius' J. Anal. Chem.*, 2000, **368**, 638–640.